ACS APPLIED MATERIALS & INTERFACES

Research Article

www.acsami.org

Solution-Based Synthesis and Low-Temperature Transport Properties of $CsBi_4Te_6$

Anuja Datta and George S. Nolas*

Department of Physics, University of South Florida, Tampa, Florida 33620, United States

ABSTRACT: The thermoelectric material $CsBi_4Te_6$ was synthesized in nanometer thin flake-like form by a low temperature solvothermal approach. The crystals were then densified by spark plasma sintering (SPS), resulting in a polycrystalline specimen with layered and partially orientated grains. The orientation of the $CsBi_4Te_6$ flakes reflects the anisotropic crystal structure of the material aided by the unidirectional pressure during SPS. Hall, resistivity, Seebeck coefficient, and thermal conductivity was measured on the polycrystalline specimen in evaluating the potential of this approach for thermoelectric applications.

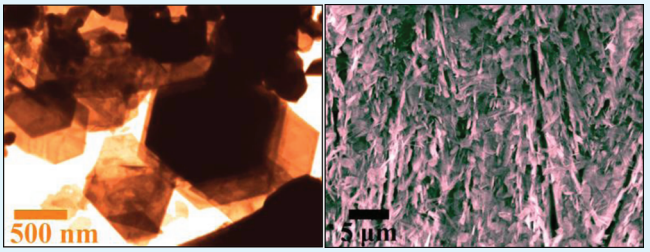

KEYWORDS: *cesium bismuth telluride, layered structure, solvothermal synthesis, spark plasma sintering, thermoelectric properties, Hall measurement*

INTRODUCTION

Recent focus in thermoelectric (TE) materials research is on new materials and new synthetic approaches.[1−4] Although $Bi_{2-x}Sb_xTe_{3-y}Se_y$ alloys[5] remain the material of choice for cooling applications, there have been several materials that have demonstrated superior TE properties.[1−9] $CsBi_4Te_6$ is one such promising TE material.[10] It possesses a relatively high TE figure of merit, $ZT = (S^2/(\rho\kappa))T$, where S is the Seebeck coefficient, ρ is the electrical resistivity, and κ is the thermal conductivity ($\kappa = \kappa_e + \kappa_L$, where κ_e and κ_L are the electronic and lattice contributions, respectively) below room temperature. Since first reported by Chung et al.,[10] research on the synthesis and TE properties of $CsBi_4Te_6$ and its doped counterparts have been undertaken.[11−18] Structurally, $CsBi_4Te_6$ possess a layered, anisotropic structure composed of anionic $[Bi_4Te_6]$ layers alternating with layers of Cs crystallizing in a monoclinic system.[10,11,13] The $[Bi_4Te_6]$ layers are strongly anisotropic therefore $CsBi_4Te_6$ crystals are typically needlelike in appearance as observed for the single crystals and bulk polycrystalline specimens prepared by solid-state synthetic approaches.[10,11,13] The highly anisotropic crystal growth habit and electronic structure of $CsBi_4Te_6$ also makes this material an important candidate for an investigation into the structure−property relationships at different length-scales and dimensions. In order to fabricate TE materials on a large scale, it is necessary to adopt low-cost, simple, morphology-controlled synthetic approaches in meeting the need of both specimen quality and yield. These are characteristics of wet-chemical growth strategies, where size and morphology control of the crystals are possible.[19−22] No previous report is available on the solution phase synthesis of $CsBi_4Te_6$, presumably because of the intricate chemistry involved in controlling the stoichiometry of the $CsBi_4Te_6$ phase.[11]

In the present work, we report on the first solution-based synthesis of $CsBi_4Te_6$ crystals. We present the structural and TE characterization of this material after consolidation, and discuss the results in terms of potential for TE applications. Keeping in mind the challenge in synthesizing ternary $CsBi_4Te_6$ by a solution-phase approach, and its anisotropic crystal structure, this work illustrates the versatility of utilizing bottom-up processing for the preparation of complex TE materials.

EXPERIMENTAL SECTION

A low temperature solvothermal process was adopted for the synthesis of $CsBi_4Te_6$ crystals. Cesium acetate ($CsCH_3COO$ 99%, Acros Organics), bismuth nitrate ($Bi(NO_3)_3{\cdot}5H_2O$ 99.99%, Alfa Aesar), and sodium tellurite (Na_2TeO_3 99.9%, Alfa Aesar) were used as the Cs, Bi and Te sources, respectively. Tetraethyleneglycol (TetraEG 99%, Acros Organics) was used as the solvent and sodium borohydride ($NaBH_4$, Fisher Scientific) was used as the reducing agent. In a typical mode of solvothermal synthesis, stoichiometric quantities of $Bi(NO_3)_3{\bullet}5H_2O$ (0.5 mmol) and Na_2TeO_3 (0.75 mmol) as per the unit formula of $CsBi_4Te_6$ were taken with an excess amount of $CsCH_3COO$ (1.2 mmol) in a custom-built PTFE chamber filled with TetraEG up to 80% of the volume of the container (45 mL in volume in total). The whole mixture was ultrasonicated for ∼30 min, upon which the solution turned milky white. An appropriate amount of $NaBH_4$ (0.1 g) was quickly added to the solution and stirred to promote homogeneity. The solution turned black gradually and effervescence indicated the initiation of the reaction. The Teflon chamber was then tightly sealed, put in a custom-built stainless steel chamber and sealed. The chamber was put in a preheated oven at 200 °C for 16 h for completion of the reaction. At the end of the reaction,

Received: October 14, 2011
Accepted: January 10, 2012
Published: January 10, 2012

the steel chamber was air-cooled to room temperature. The dark gray product was collected by centrifugation and washed several times with water and ethanol to remove any unreacted chemicals. Finally, the product was dried under vacuum for 6 h before it was collected and ground to powder. Each synthesis yielded ~0.3 g of $CsBi_4Te_6$ crystals. Approximately 2 g of $CsBi_4Te_6$ crystals were synthesized for densification. Densification was achieved by Spark Plasma Sinter (SPS) using a Thermal Technology LLC, model 25−10 at 100 MPa and 200 °C under vacuum with a 10 min hold time using 20 mm diameter graphite die and punches. A temperature ramping rate of 100 °C/min resulted in a pellet with a density of ~82% of the theoretical density of bulk $CsBi_4Te_6$. A higher temperature and temperature ramping rate were avoided due to rapid loss of volatile Cs from $CsBi_4Te_6$ structure.

The as synthesized $CsBi_4Te_6$ crystals and SPS densified polycrystalline $CsBi_4Te_6$ were characterized by X-ray diffraction (XRD, Bruker AXS D8 with Lynx Eye position sensitive detector), scanning electron microscopy (SEM, JEOL JSM 6390 LV), and transmission electron microscopy (TEM, FEI Tecnai F20 S-Twin TEM). Energy-dispersive X-ray spectroscopy (EDS) spectra on several crystals was obtained by a Tecnai F20 apparatus operated at an accelerating voltage of 300 kV with a point-to-point resolution of 2 Å attached to the TEM, and EDS of the SPS densified specimen was obtained on an Oxford Instruments INCAX sight attached to the SEM. The densified specimen was cut using a wire saw into 0.5 mm × 2 mm × 5 mm parallelepipeds for room temperature Hall measurements, and 2 mm × 2 mm × 5 mm parallelepipeds for temperature dependent four-probe resistivity, ρ, steady-state Seebeck Coefficient (gradient sweep method), S, and thermal conductivity, κ, measurements from 12 to 300 K.[23] The measurements were conducted in a custom radiation-shielded vacuum probe with uncertainties of 4, 6, and 8% for ρ, S, and κ measurements, respectively. Electrical contacts to the specimens were made by soldering directly to nickel-plated surfaces using standard techniques, and thermal contacts were made using Stycast epoxy. Room-temperature four-probe Hall measurements were conducted at multiple positive and negative magnetic fields, up to 1T to eliminate voltage probe misalignment effects, using a custom-built voltage probe with 10% uncertainty.

RESULTS AND DISCUSSION

The concentration of $CsCH_3COO$ in the precursor solution was found to be critical in controlling the purity of the $CsBi_4Te_6$ phase. The very slow reaction rate of $CsCH_3COO$ and exceptionally high thermodynamic stability of Bi_2Te_3 essentially prevents formation of $CsBi_4Te_6$. Hence, when a stoichiometric amount of $CsCH_3COO$ was used, Bi_2Te_3 was the dominant phase. On optimization of the precursor concentrations, pure $CsBi_4Te_6$ was obtained for a 9.6 times excess molar concentration of $CsCH_3COO$ instead of the stoichiometric ratio of the constituents. This chemically synthesized approach for $CsBi_4Te_6$ had good reproducibility and was stable in air. A possible reaction process for the formation of $CsBi_4Te_6$ is as follows:

$$CsCH_3COO + Na_2TeO_3 + NaBH_4 \rightarrow Cs_2Te + NaHCO_3 + BH_3 + H_2 \quad (1)$$

$$Bi(NO_3)_3{\cdot}5H_2O + Na_2TeO_3 + NaBH_4 \rightarrow Bi_2Te_3 + NaNO_3 + BH_3 + H_2 \quad (2)$$

$$Cs_2Te + Bi_2Te_3 + NaBH_4 \rightarrow CsBi_4Te_6 + BH_3 + H_2 \quad (3)$$

The XRD patterns of crushed and powdered $CsBi_4Te_6$ crystals and the densified specimen are shown in Figure 1. The XRD

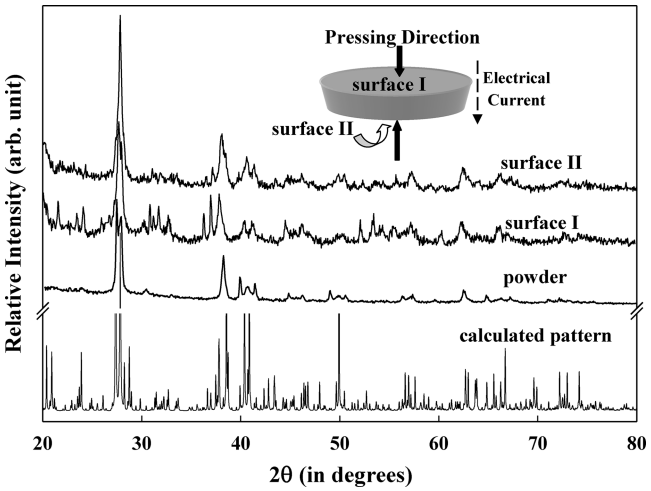

Figure 1. XRD patterns of the as-synthesized $CsBi_4Te_6$ and the two surfaces of the densified pellet in comparison to the calculated XRD pattern. The inset shows a schematic diagram indicating the relationship between the SPS pressing direction and the surfaces from which XRD spectra were taken.

patterns before and after SPS are compared with that of a calculated $CsBi_4Te_6$ pattern following the Fractional Atomic Coordinate data in ref 11. As observed from Figure 1, the XRD pattern of the crystals can be well indexed to monoclinic $CsBi_4Te_6$ crystallized in $C2/m$ (No. 12) space group.[11] The XRD spectra of the densified specimen were obtained from both surfaces of the pellet, referred to as surface I and surface II in the inset of Figure 1. Surface I refers to the side of the pellet through which the pulsed DC current entered into the material during SPS and the other side is referred to as surface II. After SPS, the XRD patterns of the specimen are consistent with the calculated $CsBi_4Te_6$ pattern, however, the intensities of the dominant peaks between 20 and 40° 2θ are somewhat different between surfaces I and II, suggesting the presence of texturing. Consolidation of the highly anisotropic TE compounds, particularly those with layered crystal structures, may often result in alignment of the grains.[24−28] The nature of this alignment may change and even become absent inside the specimen from the pressing surfaces.[24] It was observed by Chung et al.[13] that in highly oriented $CsBi_4Te_6$ needle-shaped crystals, the transport properties vary significantly along the primary crystallographic directions, and hence controlling the texture may lead to favorable transport properties.

Figure 2 shows TEM images of the solvothermally synthesized $CsBi_4Te_6$ crystals. Polygonal flakelike structures were obtained as observed from the low resolution TEM image in Figure 2a. The length of the sides of the polygonal crystals is in the range of 500 nm to 2 μm, whereas the thicknesses are of the order of tens of nanometers. The transparency of the $CsBi_4Te_6$ crystals to the electron beam was understood from the apparent visibility of the superimposed flakes (Figure 2a) and is due to the small thicknesses of the flakes as compared to the length and the width of the crystals. The presence of wavy contrast bands in the crystals are due to stress resulting from the stretching of the thin flakes on to the carbon film of the Cu TEM grid. The presence of stress bands have been observed for other low dimensional nanostructures of similar thickness.[29] Uninterrupted and sharp lattice fringes in the $CsBi_4Te_6$ flakes signifies high crystallinity (Figure 2b). The calculated lattice fringe spacing (0.34 nm) is equivalent to the Cs - Te distance in

dx.doi.org/10.1021/am201411g | ACS Appl. Mater. Interfaces 2012, 4, 772−776

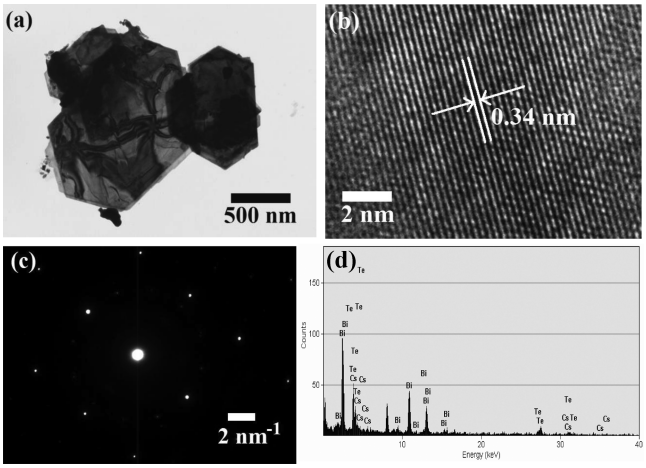

Figure 2. (a) Low-resolution TEM image of $CsBi_4Te_6$ crystals showing the thin platelike morphology. Wavy black bands in the image of the crystal are generated from stress in the thin plates. (b) High-resolution TEM (HRTEM) image showing the lattice planes in a crystal. The lattice fringe spacing is also shown. (c) Selected area electron diffraction pattern from an individual crystal, indicating a single crystal. (d) EDAX spectrum from a $CsBi_4Te_6$ single crystal under TEM showing the presence of Cs, Bi, and Te in the appropriate ratio.

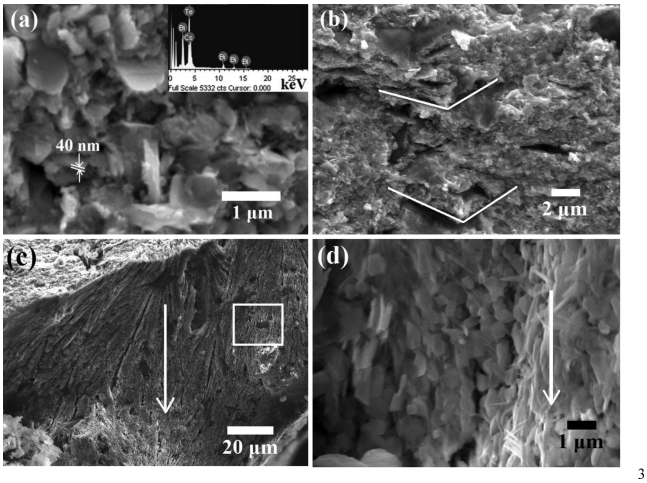

Figure 3. SEM images of a fractured surface of $CsBi_4Te_6$ after densification from (a, b) surface I and (c, d) surface II. (a) Higher-magnification SEM image indicating that the specimen is composed of thin plates of $CsBi_4Te_6$ of ~40 nm in thickness. The inset shows a representative EDS spectrum collected from the surface that indicates an excess of Bi on this surface. (b) Low-magnification SEM image indicating the presence of layered texturing (shown with white lines) that suggests orientation in the specimen. (c) Low-resolution SEM image also showing the texturing. (d) Magnified image of the area indicated in c shows that the specimen is composed of oriented plates of $CsBi_4Te_6$. The arrows indicate the pressing direction during SPS.

$CsBi_4Te_6$.[11,12] Figure 2c shows the selected area electron diffraction pattern recorded from a single $CsBi_4Te_6$ flake. Linear diffraction patterns obtained over several $CsBi_4Te_6$ crystals indicated the flakes were single crystals. The EDS spectrum obtained from a single $CsBi_4Te_6$ flake indicates that the constituent elements are in the stoichiometric ratio, to within the accuracy of EDS.

After SPS, the $CsBi_4Te_6$ specimen was investigated by SEM on fractured surfaces. There was apparent growth of the $CsBi_4Te_6$ flakes after densification, as observed from SEM analysis (Figure 3a). The specimen was composed of randomly oriented intergrown $CsBi_4Te_6$ flakes several micrometers long and approximately 40 nm thick. The EDS spectra on these surfaces indicate a Cs:Bi:Te ratio of approximately 1:4.2:6, that is, a slightly higher Bi content after densification. Although no impurities were detected in the $CsBi_4Te_6$ flakes, potential surface impurities (such as OH groups) in trace quantities may affect the densification process as well as the transport properties measurements. A low-resolution SEM image of the surface (Figure 3b) shows the local presence of layering in the specimen (indicated by the solid angles) probably developed because of the partial alignment of the $CsBi_4Te_6$ flakes during SPS processing. In another area of the specimen, the alignment of the $CsBi_4Te_6$ crystals is clearly visible (Figure 3c). The alignment of the flakes are perpendicular to the pellet surfaces, i.e., parallel to the direction at which pressure and current are applied (shown by an arrow) during SPS. Closer observation (the area marked with a rectangle) confirms that in some areas there is reasonable alignment of the $CsBi_4Te_6$ flakes along the pressing direction.

Figure 4a–c shows the low-temperature transport properties of polycrystalline $CsBi_4Te_6$ measured on a rectangular piece cut along the diameter of the pellet (perpendicular to the pressing direction). Room temperature Hall data measured in the same direction indicated n-type conductivity with a carrier concentration (n) of 2×10^{18} cm^{-3}. This n value for our $CsBi_4Te_6$ specimen is an order of magnitude lower than that of previous reports.[10,11,13] Primarily undoped $CsBi_4Te_6$ shows p-type conductivity as has been observed for polycrystals prepared by solid-state processes,[10,11,13] however, n-type conductivity in $CsBi_4Te_6$ was observed when measured along the c-axis (perpendicular to the $a-b$ plane of the ingot containing oriented needle-shaped $CsBi_4Te_6$ crystals).[13] Our polycrystalline $CsBi_4Te_6$ specimen had n-type conduction and thus was compared to bulk data measured along the c-axis[13] (Figure 4). We note that room temperature S and ρ measurements parallel and perpendicular to the pressing direction resulted in similar values. In Figure 4 Bi-doped $CsBi_4Te_6$ data are shown for comparison since our polycrystalline $CsBi_4Te_6$ specimen is slightly Bi rich after SPS densification (from EDS analysis). The polycrystalline specimen shows a decreasing ρ (Figure 4a) with decreasing temperature from 300 K to 12 K. The ρ values at all temperatures are higher than that of $CsBi_4Te_6$ single crystals measured along the c-axis (Figure 4a).[13] This is presumably due to grain-boundary scattering in addition to the effects of porosity. The presence of porosity typically increases ρ and lowers κ simultaneously due to the added scattering at the pore sites.[30−33] To understand the role of porosity in increasing ρ in our polycrystalline $CsBi_4Te_6$ specimen we calculated the porosity corrected ρ values using the Maxwell−Eucken expression[32,33]

$$\rho_{\text{correct}} = \rho_{\text{porous}} \frac{1 - \varphi}{1 + \beta\varphi} \quad (4)$$

where ρ_{correct} is the corrected ρ for a 100% dense bulk medium, ρ_{porous} is the effective ρ in the measured porous medium, φ is the degree of porosity described by a fraction between 0 and 1, and β is the correction factor typically with a value between 1.0 and 3.0 when the shape of the pores are spherical or nearly spherical. Equation 4 can also be extended to calculate the porosity corrected κ (κ_{correct}) by replacing the terms ρ_{correct} and

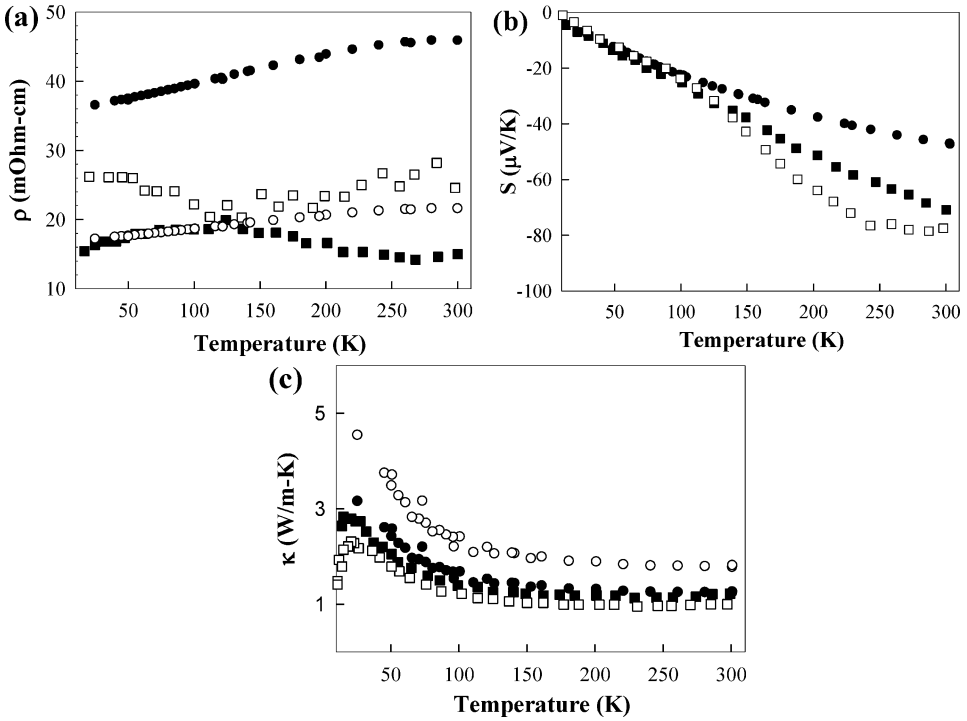

Figure 4. Low-temperature (a) resistivity, (b) Seebeck coefficient, and (c) thermal conductivity of polycrystalline $CsBi_4Te_6$ (●) shown in comparison to undoped (■) and Bi doped bulk $CsBi_4Te_6$ (□) from ref 13. The porosity corrected resistivity and thermal conductivity values (○) using the Maxwell−Eucken expression are also shown.

ρ_{porous} with $1/\kappa_{correct}$ and $1/\kappa_{porous}$, respectively. Assuming a nearly spherical pore shape we set β to 2.[33] After this porosity correction, the ρ values for the polycrystalline $CsBi_4Te_6$ specimen are more consistent with that of the bulk $CsBi_4Te_6$ (Figure 4a). Figure 4b shows the S values for the polycrystalline $CsBi_4Te_6$ specimen in comparison to the undoped and Bi doped oriented $CsBi_4Te_6$ crystal data.[13] The polycrystalline specimen has a relatively low S of ≈ -47 μV/K compared to the value measured on $CsBi_4Te_6$ needles. Low S values may occur due to the random orientation of the grains in spite of some local texturing. The negative S values for all temperatures corroborate the Hall data that indicated electrons to be the majority carriers. Our $CsBi_4Te_6$ polycrystalline specimen shows a similar temperature dependence and κ values compared to that of the bulk (Figure 4c). Keeping in mind that κ in TE materials may also be affected by porosity, we used eq 4, as described above, to calculate $\kappa_{correct}$ (Figure 4c). The κ values thus obtained are similar to that previously reported.[10] In addition, the large room-temperature ρ values infer that the electronic contribution to κ is negligible, and thus the observed κ of polycrystalline $CsBi_4Te_6$ can be attributed almost entirely to κ_L.

Effectively, the chemically synthesized and SPS densified polycrystalline $CsBi_4Te_6$ specimen resulted in low ZT values as was also observed for $CsBi_4Te_6$ measured along the c-axis.[13] Chung et al.[13] indicated that that TE properties of $CsBi_4Te_6$ are highly dependent on direction. In polycrystalline specimens, a random orientation of the grains presumably results in degradation of the TE properties. Assuming that grain orientation can be controlled by SPS, as has been accomplished in other materials,[33−36] the TE properties of chemically synthesized $CsBi_4Te_6$ can be improved.

CONCLUSIONS

We have synthesized $CsBi_4Te_6$, an important low-temperature TE material, as nanometer thick polygonal flakes of lengths varying from 500 nm to 2 μm using a solvothermal approach. The $CsBi_4Te_6$ phase was obtained via reaction of cesium acetate used in excess with bismuth nitrate, sodium tellurite and sodium borohydride in tetraethyleneglycol solvent at 200 °C after 16 h. The $CsBi_4Te_6$ crystals were densified via SPS resulting in a random dispersion of 40 nm thick $CsBi_4Te_6$ flakes with some signature of layering and texturing in the polycrystalline specimen. Analyses revealed a Bi rich composition with partial orientation of the $CsBi_4Te_6$ flakes after SPS processing. Room-temperature Hall measurements indicated n-type conductivity. Low-temperature ρ, S, and κ data were compared to that of n-type $CsBi_4Te_6$ measured along the c-axis.[13] The solution-based synthesis of $CsBi_4Te_6$ revealed the flexibility of this approach in preparing complex TE materials, and offers a platform for expanding the investigation of the fundamental structural and transport properties of this and other similar materials with potential for TE applications.

AUTHOR INFORMATION

Corresponding Author

*E-mail: gnolas@usf.edu.

ACKNOWLEDGMENTS

This work is supported by the U.S. Army Medical Research and Materiel Command under Grant W81XWH-07-1-0708 and the National Science Foundation under Grant No. CBET-0932526. We thank Daniela Fredrick of Thermal Technology, LLC, for SPS of $CsBi_4Te_6$ crystals.

REFERENCES

(1) Dresselhaus, M. S.; Chen, G.; Tang, M. Y.; Yang, R.; Lee, H.; Wang, D.; Ren, Z.; Fleurial, J. −P.; Gogna, P. *Adv. Mater.* **2007**, *19*, 1043.
(2) Kanatzidis, M. G. *Chem. Mater.* **2010**, *22*, 648.
(3) Sootsman, J. R.; Chung, D. Y.; Kanatzidis, M. G. *Angew. Chem., Int. Ed.* **2009**, *48*, 8616.
(4) Minnich, A. J.; Dresselhaus, M. S.; Ren, Z. F.; Chen, G. *Energy Environ. Sci.* **2009**, *2*, 466.
(5) Nolas, G. S.; Sharp, J.; Goldsmid, H. J. *Thermoelectrics: Basic Principles and New Materials Developments*; Springer: New York, 2001.
(6) Snyder, G. J.; Toberer, E. S. *Nat. Mater.* **2008**, *7*, 105.
(7) Vineis, C. J.; Shakouri, A.; Majumdar, A.; Kanatzidis, M. G. *Adv. Mater.* **2010**, *22*, 3970.
(8) Li, J.-F.; Liu, W.-S.; Zhao, L.-D.; Zhou, M. *NPG Asia Mater.* **2010**, *2*, 152.
(9) Lan, Y.; Minnich, A. J.; Chen, G.; Ren, Z. *Adv. Funct. Mater.* **2010**, *20*, 357.
(10) Chung, D.-Y.; Hogan, T.; Brazis, P.; Rocci-Lane, M.; Kannewurf, C.; Bastea, M.; Uher, C.; Kanatzidis, M. G. *Science* **2000**, *287*, 1024.
(11) Chung, D.-Y.; Hogan, T.; Rocci-Lane, M.; Brazis, P.; Ireland, J. R.; Carl R. Kannewurf, C.; Bastea, M.; Uher, C.; Kanatzidis. *J. Am. Chem. Soc.* **2004**, *126*, 6414.
(12) Hsu, K.-F.; Chung, D.-Y.; Lal, S.; Mrotzek, A.; Kyratsi, T.; Hogan, T.; Kanatzidis, M. G. *J. Am. Chem. Soc.* **2002**, *124*, 2410.
(13) Chung, D.-Y.; Mahanti, S. D.; Chen, W.; Uher, C.; Kanatzidis, M. G. *Mater. Res. Soc. Symp. Proc.* **2004**, *793*, S6.1.1.
(14) Hsu, K.-F.; Lal, S.; Hogan, T.; Kanatzidis, M. G. *Chem. Commun.* **2002**, 1380.
(15) Greanya, V. A.; Tonjes, W. C.; Liu, R.; Olson, C. G.; Chung, D.-Y.; Kanatzidis, M. G. *Phys. Rev. B* **2002**, *65*, 205123.
(16) Larson, P.; Mahanti, S. D.; Chung, D.-Y.; Kanatzidis, M. G. *Phys. Rev. B* **2002**, *65*, 045205.
(17) Luo, W.; Souza de Almeida, J.; Osorio-Guillen, J. M.; Ahuja, R. *J. Phys. Chem. Solids* **2008**, *69*, 2274.
(18) Lykke, L.; Iversen, B. B.; Madsen, G. K. H. *Phys. Rev. B* **2006**, *73*, 195121.
(19) Martin, J.; Nolas, G. S.; Zhang, W.; Chen, L. *Appl. Phys. Lett.* **2007**, *90*, 222112.
(20) Martin, J.; Wang, L.; Chen, L.; Nolas, G. S. *Phys. Rev. B* **2009**, *79*, 115311.
(21) Datta, A.; Paul, J.; Kar, A.; Patra, A.; Sun, Z.; Chen, L.; Martin, J.; Nolas, G. S. *Cryst. Growth Des.* **2010**, *10*, 3983.
(22) Ozin, G. A. *Adv. Mater.* **1992**, *4*, 615.
(23) Martin, J.; Nolas, G. S.; Wang, H.; Yang, J. *J. Appl. Phys.* **2007**, *102*, 103719.
(24) Medlin, D. L.; Snyder, G. J. *Curr. Opin. Colloid Interface Sci.* **2009**, *14*, 226.
(25) Gonzalez, E. J.; Blendell, J. E.; Cline, J. P.; Ritter, J. J.; Maruthamuthu, P.; Nelson, E. H.; Horn, S.B.. *J. Mater. Res.* **1998**, *13*, 766.
(26) Seo, J.; Lee, C.; Park, K. *J. Mater. Sci.* **2000**, *35*, 1549.
(27) Fan, X. A.; Yang, J. Y.; Chen, R. G.; Zhu, W; Bao, S. Q. *J. Appl. Phys.* **2007**, *101*, 113707.
(28) Böttner, H.; Ebling, D. G.; Jacquot, A.; König, K.; Kirste, L.; Schmidt. *J. Phys. Status Solidi* **2007**, *1*, 235.
(29) Wang, Z. L. *Annu. Rev. Phys. Chem.* **2004**, *55*, 159.
(30) Lee, H.; Vashaee, D.; Wang, D. Z.; Dresselhaus, M. S.; Ren, Z. F. *J. Appl. Phys.* **2010**, *107*, 094308.
(31) Adachi, J.; Katayama, M.; Kurosaki, K.; Uno, M.; Yamanaka, S. *J. Nucl. Mater.* **2008**, *376*, 83.
(32) Adachi, J.; Kurosaki, K.; Uno, M.; Yamanaka, S. *J. Alloys Compd.* **2007**, *432*, 7.
(33) Scheele, M.; Oeschler, N.; Veremchuk, I.; Reinsberg, K.-G.; Kreuziger, A.-M.; Kornowski, A.; Broekaert, J.; Klinke, C.; Weller, H.; Chen, G. *ACS Nano* **2010**, *4*, 4283.
(34) Ohsugi, I. J.; Kojima, T.; Sakata, M.; Yamanashi, M.; Nishida, I. A. *J. Appl. Phys.* **1994**, *76*, 2235.
(35) Ge, Z.-H.; Zhang, B.-P.; Shang, P.-P.; Li, J. -F. *J. Mater. Chem.* **2011**, *21*, 9194.
(36) Noudem, J. G. *J. Eur. Ceram. Soc* **2009**, *29*, 2659.